

## Shape Evolution of Single-Crystalline Iron Oxide Nanocrystals

Jinwoo Cheon,\* Nam-Jung Kang,† Sang-Min Lee, Jae-Hyun Lee, Ji-Hyun Yoon, and Sang Jun Oh‡

Department of Chemistry, Yonsei University, Seoul 120-749, Korea

Received September 25, 2003; E-mail: jcheon@alchemy.yonsei.ac.kr

The design and synthesis of architectural nanocrystals have been among the important research topics of nanoscience due to their unique size and shape-dependent phenomena.<sup>1</sup> Therefore, systematic directions for synthetic methods and an understanding of the mechanisms by which the size and shape of the nanocrystals can be controlled are of particular interest. Recent demonstration of a variety of novel shapes such as rods (CdSe),<sup>2a</sup> branched rods (CdS, CdTe, MnS),<sup>2b-d</sup> stars (PbS),<sup>2c</sup> and tetrahedrons (Pt, CdS)<sup>2f-h</sup> developed by us and others suggest that the role of capping ligand plays a critical role in the shape-control processes.<sup>3</sup>

While shape-control studies are actively being pursued on the semiconductor and metal nanocrystals,<sup>2,3</sup> little work exists for magnetic metal oxide system despite their unique nanomagnetism and important technological applications including magnetic information storage, biological tags, and ferrofluids.<sup>4</sup> Recent successful synthetic studies of iron oxide nanocrystals have mostly focused on 0-D spheres.<sup>5</sup> Multistep synthetic processes or the use of multireagents (e.g., additional oxidant) was typically required in these methods. Although iron oxide nanopyramids via a polymer-assisted synthetic approach has been reported, their structural characterizations were not clearly elucidated.<sup>6</sup>

In this communication, we report the shape evolutions of magnetic iron oxide nanocrystals utilizing a simple one-step synthesis without any additional reagents such as (CH<sub>3</sub>)<sub>3</sub>NO.<sup>5b</sup> We also examine the roles of parameters critical to the size- and shape-guiding processes.

Structurally well-defined iron oxide nanocrystals with shapes consisting mainly diamonds, triangles, and spheres were obtained from the thermal decomposition of Fe(CO)<sub>5</sub> in a hot solution (180 °C) containing capping ligand (dodecylamine (DDA)) under aerobic condition with a precursor-to-capping ligand molar ratio of 1:1.<sup>7</sup> During this thermolysis and air oxidation process, the initial orange color of the solution changed to deep red-brown. After 9 h, the resulting solution was separated and analyzed. TEM analysis (Figure 1) shows a mixture of diamond- (~40%), sphere- (~30%), and triangle-shaped (~30%) nanocrystals all similar in size (~12 nm). HRTEM images illustrate that these nanocrystals are high-quality single-crystalline maghemite (γ-Fe<sub>2</sub>O<sub>3</sub>) (Figure 1B–E). The interplanar distances of diamond- and sphere-shaped nanocrystals are 4.92, 2.08, and 2.95 Å along the <110> zone axis with separation angles of 70° and 90° between the planes, which are consistent with known values for the {111}, {040}, and {202} planes of γ-Fe<sub>2</sub>O<sub>3</sub>, respectively (Figure 1B, C).<sup>8</sup> The structure of the diamond-shaped nanocrystals is a dodecahedron truncated along the [111] and [100] directions (Figure 1E). The spherical nanocrystals possess weak facets similar to those of the diamond structures, but they are not as pronounced (Figure 1C). In triangular nanocrystals, the lattice plane distance of 2.96 Å in the {220} planes along the <111> zone axis (Figure 1D) suggests that it is a nanoprism highly truncated along the {111} face of a tetrahedron. X-ray photoelectron

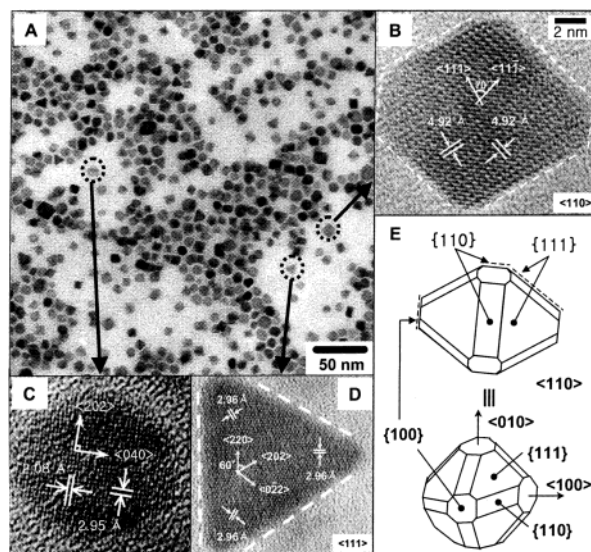


**Figure 1.** (A) TEM images of ~12 nm γ-Fe<sub>2</sub>O<sub>3</sub> nanocrystals and HRTEM images of (B) diamond, (C) sphere, (D) triangle shapes and (E) 3-D and 2-D model projected along <110> direction of a diamond structure.

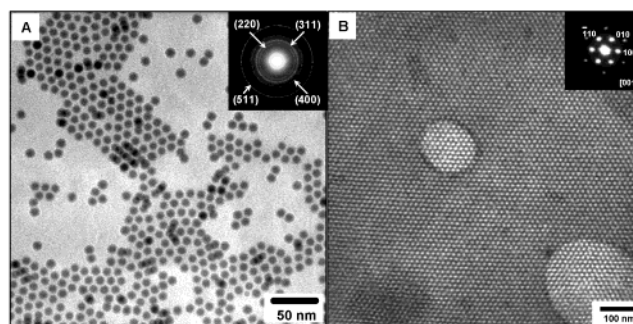


**Figure 2.** (A) TEM image of γ-Fe<sub>2</sub>O<sub>3</sub> spherical nanocrystals after the shape-selection process and (B) hexagonal close-packed superlattices of γ-Fe<sub>2</sub>O<sub>3</sub> obtained by slow evaporation of a solvent.

spectroscopic data show peaks at 710.5 and 723.4 eV which are in good agreement with the known values of Fe(2p<sub>3/2</sub>) and Fe(2p<sub>1/2</sub>) of γ-Fe<sub>2</sub>O<sub>3</sub> respectively.<sup>8a</sup> Further X-ray absorption and Raman spectroscopic analyses of the sample confirm that these nanocrystals are indeed γ-Fe<sub>2</sub>O<sub>3</sub>.<sup>7,8</sup>

Spherical nanocrystals were isolated from the mixtures via a simple precipitation method. TEM image shows monodisperse nanocrystals of 12 nm ( $\sigma = 4.6\%$ ) (Figure 2A), and these nanocrystals can further be assembled into well-ordered three-dimensional (3-D) hexagonal close-packed superlattices upon recrystallization by slow evaporation of a high-boiling point solvent such as toluene (Figure 2B). This also demonstrates the high uniformity of the nanocrystals.

The shape and size of γ-Fe<sub>2</sub>O<sub>3</sub> nanocrystals can be further tuned by adjusting growth parameters. When the molar ratio of the

\* Current address: Samsung Electronics, Yong-In 449-711, Korea.

‡ Korea Basic Science Institute, Daejeon 305-333, Korea.

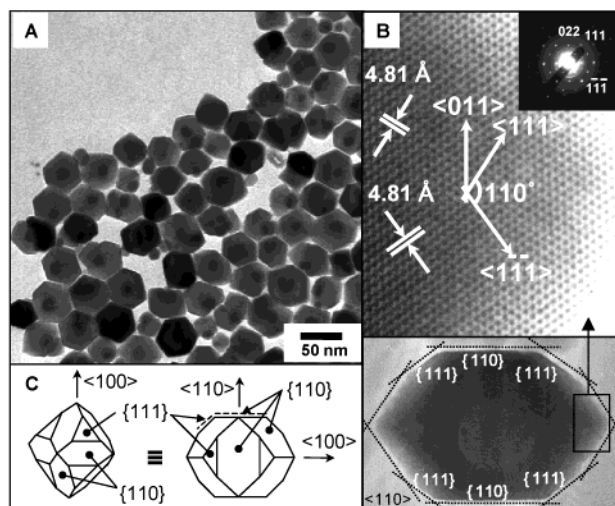


**Figure 3.** (A) TEM image of hexagon-shaped  $\gamma$ -Fe<sub>2</sub>O<sub>3</sub> nanocrystals obtained at high capping-ligand concentration. (B) HRTEM images of fringe patterns of a hexagon. (C) 3-D and 2-D model projected along  $\langle 110 \rangle$  direction.

capping molecule (DDA) to the precursor (Fe(CO)<sub>5</sub>) is increased to 10:1, much larger nanocrystals are obtained. The TEM image shows hexagon-shaped nanocrystals on the order of 50 nm ( $\sigma = 10.4\%$ ) (Figure 3A) and some appearing aligned like a “necklace”-type pattern due to their strong dipolar magnetic interactions.<sup>7</sup>

The HRTEM image shows that the interplanar distance of {111} planes is 4.81 Å with their separation angle of 110° along the  $\langle 110 \rangle$  zone axis with the electron diffraction patterns also being consistent with those of a  $\gamma$ -Fe<sub>2</sub>O<sub>3</sub> structure (Figure 3B). Careful examination of this hexagon structure indicates that it is, in fact, a decagon under 2-D projection with dominant facets of {111} and {110} faces (Figure 3B, C). Its 3-D structure is a {111} truncated dodecahedron with complete growth in [100] directions.

The typical structure of a seed for the inverse spinel structure of  $\gamma$ -Fe<sub>2</sub>O<sub>3</sub> is based on an fcc model with three low-energy surfaces {100}, {110}, and {111}.<sup>9</sup> It is possible that highly {111} face-developed diamonds and prisms are obtained when the majority of the alkylamine ligand is preferentially bound to the highest-energy {111} surfaces under low ligand concentration. As the amount of the ligand increases significantly, not only does the {111} surface show saturated surface coverage, the surface of next highest in energy, the {110} surface, is now coordinated by the capping ligand, resulting in hexagon shapes with both the {110} and {111} surfaces well developed.

Smaller nanocrystals were formed by utilizing the same experimental conditions with the exception of the identity of the capping ligand.  $\gamma$ -Fe<sub>2</sub>O<sub>3</sub> nanocrystals obtained by using trioctylphosphine oxide (TOPO) capping ligands instead of alkylamines are approximately 6 nm ( $\sigma = 5.1\%$ ).<sup>7</sup>

The alkylamine ligand used in this study seems to bind weakly to the metal centers on the surface of nanocrystals, while the TOPO ligand forms a much stronger bond to the crystal surface due to its high oxophilicity.<sup>10</sup> A weakly binding ligand can reversibly coordinate to the metal sites on the surface, and further growth or ripening processes are possible when sufficient amounts of alkylamine ligand are available. In fact, by increasing the amount of DDA by a factor of a 10, a mixture of large (~40 nm) and small (~10 nm) highly faceted nanocrystals is observed 9 h after the injection of the precursor. The hexagon-shaped nanocrystals grow to about 50 nm and become more monodispersed after reaction

time of 16 h. Remaining smaller nanocrystals are rare, and even some observed are very small in size (<3 nm).<sup>7</sup> These results are consistent with the Ostwald ripening process during which large crystals grow even larger at the expense of smaller nanocrystals.<sup>9</sup> In contrast, when strongly binding ligands such as TOPO are used, only small nanocrystals (~6 nm) result.

Size-dependent magnetic properties were also investigated, and 12 nm spherical nanocrystals exhibit magnetic coercivity ( $H_c$ ) of 520 Oe at 5 K, but are superparamagnetic (i.e.,  $H_c = 0$  Oe) at 300 K. Formation of iron oxide superlattices induces a slight increase of  $H_c$  to 554 and 9 Oe at 5 and 300 K, respectively. Large hexagon-shaped nanocrystals (~50 nm) exhibit  $H_c$  of 730 Oe at 5 K and ferrimagnetism with  $H_c$  of 52 Oe at 300 K.<sup>7</sup>

In a summary, shape- and size-controlled synthesis of single-crystalline maghemite ( $\gamma$ -Fe<sub>2</sub>O<sub>3</sub>) nanocrystals are performed by utilizing a solution-based one-step thermolysis method. Modulating the growth parameters—such as the type and amount of capping ligands as well as the growth time—is shown to have a significant effect on the overall shape and size of the obtained nanocrystals and on the ripening process itself. The resulting shapes of the novel structures are diverse, including slightly faceted spheres, diamonds, prisms, and hexagons, all of which are in fact truncated dodecahedron structures with different degrees of truncation along the {111}, {110}, or {100} faces. These types of studies concerning the shape evolution of nanocrystals should be valuable for further design and for greater understanding of advanced nanoscale building-block architectures.

**Acknowledgment.** This project is funded by the U.S. Department of the Navy (N62649-03-1-0008), KOSEF (1999-1-122-001-5), and National R&D Project for Nano Sci. and Tech. of Korea. We thank Prof. Kwan Kim for the Raman studies, Dr. Min Gyu Kim for XAS analyses, KBSI for TEM data, and Prof. Insung S. Choi for his kind help.

**Supporting Information Available:** XPS, XRD, XAS, Raman, SQUID, and further TEM analyses of  $\gamma$ -Fe<sub>2</sub>O<sub>3</sub> nanocrystals (PDF). This material is available free of charge via the Internet at <http://pubs.acs.org>.

## References

- (1) (a) Alivisatos, A. P. *J. Phys. Chem.* **1996**, *100*, 13226. (b) Cui, Y.; Lieber, C. M. *Science* **2001**, *291*, 851. (c) Jin, R.; Cao, Y. W.; Mirkin, C. A.; Kelly, K. L.; Schatz, G. C.; Zheng, J. G. *Science* **2001**, *294*, 1901.
- (2) (a) Peng, X.; Manna, L.; Yang, W.; Wickham, J.; Scher, E.; Kadavanich, A.; Alivisatos, A. P. *Nature* **2000**, *404*, 59. (b) Jun, Y.-W.; Lee, S.-M.; Kang, N.-J.; Cheon, J. *J. Am. Chem. Soc.* **2001**, *123*, 5150. (c) Manna, L.; Milliron, D. J.; Meisel, A.; Scher, E. C.; Alivisatos, A. P. *Nat. Mater.* **2003**, *2*, 382. (d) Jun, Y.-W.; Jung, Y.-Y.; Cheon, J. *J. Am. Chem. Soc.* **2002**, *124*, 615. (e) Lee, S.-M.; Jun, Y.-W.; Cho, S.-N.; Cheon, J. *J. Am. Chem. Soc.* **2002**, *124*, 11244. (f) Ahmadi, T. S.; Wang, Z. L.; Green, T. C.; Henglein, A.; El-Sayed, M. A. *Science* **1996**, *272*, 1924. (g) Wang, Z. L. *J. Phys. Chem. B* **2000**, *104*, 1153. (h) Pinna, N.; Weiss, K.; Sack-Kongehl, H.; Vogel, W.; Urban, J.; Pileni, M. P. *Langmuir* **2001**, *17*, 7982.
- (3) Lee, S.-M.; Cho, S.-N.; Cheon, J. *Adv. Mater.* **2003**, *15*, 441.
- (4) Cornell, R. M.; Schwertmann, U. *The Iron Oxide-Structure, Properties, Reactions, Occurrence and Uses*; VCH: Weinheim, Germany, 1996.
- (5) (a) Rockenberge, J.; Scher, E. C.; Alivisatos, A. P. *J. Am. Chem. Soc.* **1999**, *121*, 11595. (b) Hyeon, T.; Lee, S. S.; Park, J.; Chung, Y.; Na, H. B. *J. Am. Chem. Soc.* **2001**, *123*, 12798. (c) Sun, S.; Zeng, H. *J. Am. Chem. Soc.* **2002**, *124*, 8204.
- (6) Tannenbaum, R.; Reich, S.; Flenniken, C. L.; Goldberg, E. P. *Adv. Mater.* **2002**, *14*, 1402.
- (7) See Supporting Information.
- (8) (a) Fujii, T.; de Groot, F. M. F.; Sawatzky, G. A.; Voogt, F. C.; Kibma, T.; Okada, K. *Phys. Rev. B* **1999**, *59*, 3195. (b) Shmakov, A. N.; Kryukova, G. N.; Tsybulya, S. V.; Chuvilin, A. L.; Solovyeva, L. P. *J. Appl. Crystallogr.* **1995**, *28*, 141. (c) Corrias, A.; Ennas, G.; Paschina, G. *Phys. Chem. Chem. Phys.* **2000**, *2*, 1045. (d) de Faria, D. L. A.; Venancio Silva, S.; de Oliveira, M. T. *J. Raman Spectrosc.* **1997**, *28*, 873.
- (9) Sugimoto, T. *Monodispersed Particles*; Elsevier: Amsterdam, 2001.
- (10) Fe–O binding force: 390.4 kJ mol<sup>-1</sup>.

JA0387220